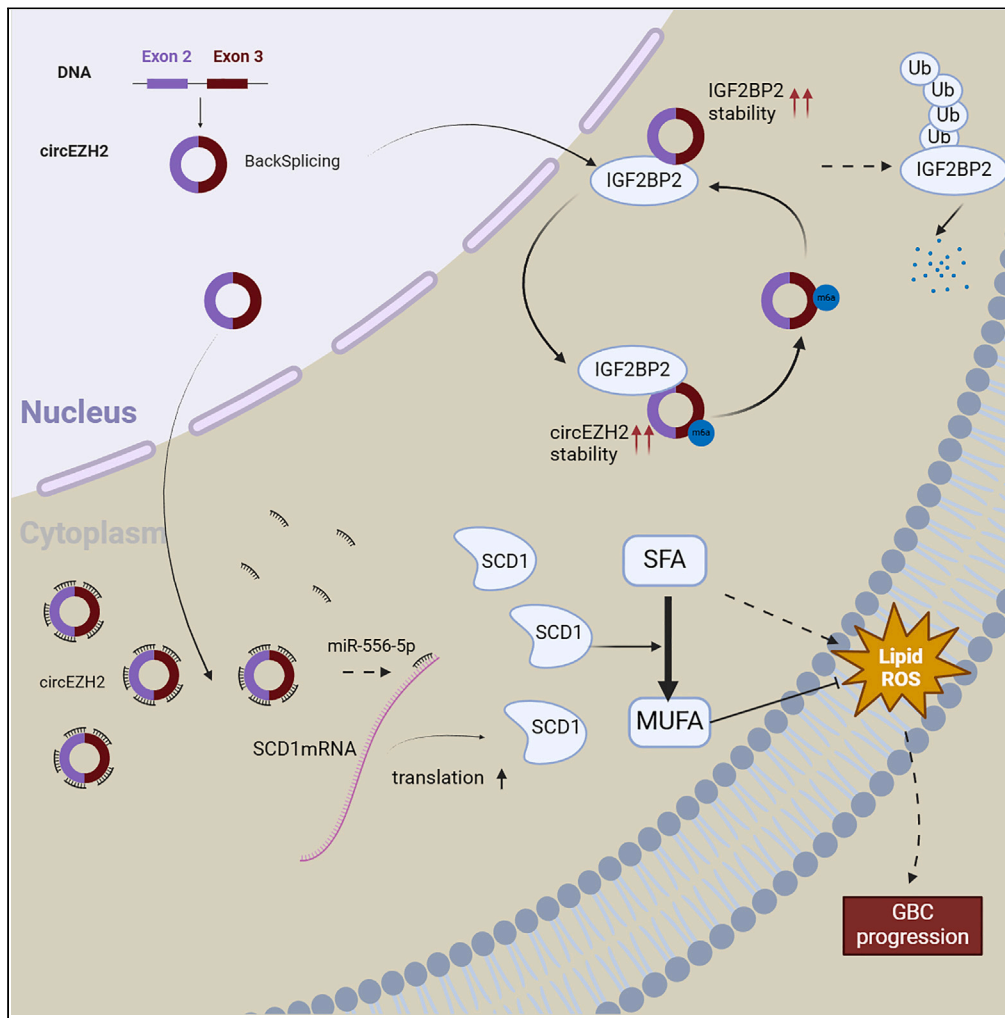**Article**

CircEZH2 promotes gallbladder cancer progression and lipid metabolism reprograming through the miR-556-5p/SCD1 axis

Huanjun Tong,
Xiaopeng Yu,
Difan Zhou, ...,
Jianhua Yu,
Shouhua Wang,
Zhaohui Tang

wangshouhua@xinhuamed.
com.cn (S.W.)
tzh1236@163.com (Z.T.)

Highlights

circEZH2 is upregulated in GBC and associated with GBC progression

circEZH2 functions as an efficient miR-556-5p sponge in GBC cells

SCD1 is a functional target of miR-556-5p in GBC cells

circEZH2 regulates GBC lipid metabolism reprograming via miR-556-5p/SCD1 axis

Article

CircEZH2 promotes gallbladder cancer progression and lipid metabolism reprogramming through the miR-556-5p/SCD1 axis

Huanjun Tong,[1,2,3,4,5,7] Xiaopeng Yu,[2,3,4,6,7] Difan Zhou,[1,5] Zhihong Shen,[1,5] Jialu Chen,[2,3,4] Yu Si,[4] Lulu Zhang,[1] Baochun Lu,[1,5] Jianhua Yu,[1,5] Shouhua Wang,[2,3,*] and Zhaohui Tang[2,3,4,8,*]

SUMMARY

Gallbladder cancer (GBC) is characterized by a high degree of malignancy and a poor prognosis. This study revealed that circEZH2 was frequently upregulated in GBC tissues and correlated with advanced tumor-node-metastasis (TNM) stage in GBC patients. *In vitro* and *in vivo* experiments confirmed that circEZH2 promoted the proliferation and inhibited the ferroptosis of GBC. Besides, this study discovered that circEZH2 regulated lipid metabolism reprogramming in GBC cells. Mechanistically, circEZH2 promotes SCD1 expression by sponging miR-556-5p in GBC cells. In addition, IGF2BP2 enhances the stability of circEZH2 in an m6A-dependent manner, while circEZH2 suppresses the ubiquitination and degradation of IGF2BP2 by binding to IGF2BP2. Taken together, our findings indicated that circEZH2, upregulated via a positive feedback loop between circEZH2 and IGF2BP2, promotes GBC progression and lipid metabolism reprogramming through the miR-556-5p/SCD1 axis in GBC. circEZH2 may serve as a potential therapeutic target for GBC.

INTRODUCTION

Gallbladder cancer (GBC) is the most common tumors of the biliary tract. It poses a major challenge in the field of oncology.[1] Despite its limited prevalence, GBC is highly aggressive and exhibits nonspecific symptoms in the early stages, which leads to delayed diagnosis and missed opportunities for optimal surgical treatment.[2] Approximately 84,695 patients worldwide died from GBC in 2020.[3] The 5-year overall survival (OS) rate of GBC patients is less than 5%.[4] The mean OS time of GBC patients is only 7.2 months.[5] Thus, there is an urgent need to clarify the molecular mechanisms underlying GBC in order to develop effective therapeutic interventions.

Circular RNAs (circRNAs) are a class of noncoding RNAs that execute many functions. In contrast to linear RNAs, circRNAs are covalently closed loops produced by backsplicing at the 3′ and 5′ ends of precursor mRNAs.[6] Due to their unique circular structure, circRNAs are resistant to degradation by exonucleases and are more stable than their linear counterparts.[7] CircRNAs were initially considered by-products or splicing errors with no effect on pre-mRNA processing, but circRNAs are now believed to have multiple functions in regulating various cellular processes.[8–10] Emerging evidence suggests that circRNAs are involved in gastric,[11] breast,[12] and prostate[13] cancer progression by acting as miRNA sponges,[12] transcription factor binding partners,[13] and protein-molecular scaffolds.[11] Our previous research identified several circRNAs that play vital biological roles in GBC, such as circFOXP1,[14] circTP63,[15] circβ-catenin,[16] and circPVT1.[17] CircEZH2 (hsa_circ_0006357), which originates from exons 2 and 3 of the EZH2 gene, was demonstrated to promote colorectal cancer cell malignant progression *in vitro* and *in vivo* via the circEZH2/miR-133b/IGF2BP2/CREB1 regulatory axis.[18] In prostate cancer, circEZH2 is a dual inhibitor of miR-363/miR-708 that subsequently downregulates the expression of EZH2.[19] However, there is still no research illuminating its role in GBC progression.

Metabolic reprogramming is one of the hallmarks of tumors.[20] Previously, the metabolic reprogramming of GBC has been mostly limited to glucose metabolism.[16] In recent years, an increasing body of attention has been given to alterations in lipid metabolism.[21–23] The intricate interplay between GBC and lipid metabolic pathways has emerged as a significant determinant of the pathogenesis of this aggressive disease. Studies have shown that lipid metabolic reprogramming involves changes in *de novo* lipogenesis, fatty acid oxidation, and lipid profiles, which jointly contribute to the malignant progression and chemotherapeutic resistance of GBC.[23] Acyl-coenzyme A (CoA) synthetase

[1]Department of Hepatobiliary Surgery, Shaoxing People's Hospital (Shaoxing Hospital, Zhejiang University School of Medicine), Shaoxing, Zhejiang, China
[2]Department of General Surgery, Xinhua Hospital, Shanghai Jiao Tong University School of Medicine, Shanghai 200092, China
[3]Shanghai Key Laboratory of Biliary Tract Disease Research, Xinhua Hospital, Shanghai Jiao Tong University School of Medicine, Shanghai 200092, China
[4]Department of Blood Transfusion, Xinhua Hospital, Shanghai Jiao Tong University School of Medicine, Shanghai 200092, China
[5]Shaoxing Key Laboratory of Minimally Invasive Abdominal Surgery and Precise Treatment of Tumour, Shaoxing, Zhejiang, China
[6]Shanghai Clinical Research Ward (SCRW), Shanghai Sixth People's Hospital Affiliated to Shanghai Jiao Tong University School of Medicine, Shanghai 200233, China
[7]These authors contributed equally
[8]Lead contact
*Correspondence: wangshouhua@xinhuamed.com.cn (S.W.), tzh1236@163.com (Z.T.)
https://doi.org/10.1016/j.isci.2024.110428

long-chain family member 4 (ACSL4), a critical isoenzyme involved in the metabolism of polyunsaturated fatty acids (PUFAs), dictates cellular sensitivity to ferroptosis. Knocking down Sirtuin 3 (SIRT3) inhibits the Akt-induced expression of ACSL4 in GBC cells. This inhibition fosters lipid peroxidation, triggering ferroptosis and subsequently suppressing the epithelial-mesenchymal transition (EMT) and invasion in GBC cells.[22] Fatty acid synthase (FASN), a key enzyme in *de novo* fatty acid synthesis, is significantly overexpressed in GBC tissues and is correlated with high histological grade. Inhibiting FASN expression at the genetic or pharmacological level can promote apoptosis and enhance sensitivity to gemcitabine by suppressing the PI3K/AKT signaling pathway in GBC cells.[23] Stearoyl-CoA desaturase 1 (SCD1) is at the crossroads of cellular lipid metabolism and plays a pivotal role in controlling the balance of saturated and monounsaturated fatty acids (MUFAs), which regulate membrane structure, energy storage, and cell signaling. Recent studies have illuminated the importance of SCD1 and its expression profile in colorectal,[24] breast,[25] and ovarian[26] cancers. However, the expression, functional role, and specific regulatory mechanisms of SCD1 in GBC remain unclear.

In this study, we identified a circRNA, circEZH2 (hsa_circ_0006357), which is closely associated with lipid metabolism, significantly upregulated in GBC tissues and correlated with advanced tumor-node-metastasis (TNM) stage. Mechanistically, we found that circEZH2 could sponge miR-556-5p, regulating the downstream expression of SCD1. This interaction alters the ratio of MUFAs to saturated fatty acids (SFAs) in GBC cells, further influencing the malignant progression of GBC cells. Additionally, we discovered that circEZH2 undergoes m6A modification, which is recognized by the m6A reading protein IGF2BP2, thereby enhancing its stability. On the other hand, circEZH2 suppresses the ubiquitination-mediated degradation of IGF2BP2 by binding to IGF2BP2, which results in a positive feedback loop to upregulate the expression of circEZH2. Taken together, our findings indicated that circEZH2, upregulated via a positive feedback loop, promotes GBC progression and lipid metabolism reprogramming through the miR-556-5p axis. Therefore, our findings suggest that circEZH2 may serve as a potential therapeutic target for GBC treatment.

RESULTS

CircEZH2 is upregulated in GBC tissues and cell lines

To explore the clinical significance of circEZH2 in GBC, we examined the expression of circEZH2 in GBC tissues using RT-qPCR. The results revealed significant upregulation of circEZH2 in GBC tissues compared to adjacent normal tissues (Figure 1A). Subsequently, based on the median relative expression level of circEZH2 in GBC tissues, patients were divided into two groups: those with high circEZH2 expression and those with low circEZH2 expression. Fisher's exact tests based on circEZH2 expression and clinical features indicated an association between high circEZH2 expression and advanced TNM stage (Table 1). Furthermore, we examined the expression levels of circEZH2 in GBC cell lines. We found that circEZH2 expression was significantly higher in the GBC-SD, NOZ, and SGC-996 cell lines than in human normal biliary epithelial cells (H69), with the highest expression observed in NOZ cells and the lowest in GBC-SD cells (Figure 1B). These results suggest that circEZH2 may promote the malignant progression of GBC.

CircEZH2 is derived from the backsplicing of exons 2 and 3 of the EZH2 gene and has a length of 253 nucleotides. The full-length sequence and the junction site were confirmed by amplification with divergent primers and subsequent detection through Sanger sequencing (Figure 1C). Due to their unique circular structure, circRNAs exhibit greater stability than mRNAs. We utilized actinomycin D to inhibit RNA synthesis in NOZ cells and measured the content of intracellular RNA to determine the stability of the RNA. We observed that the degradation rate of circEZH2 in NOZ cells was lower than that of EZH2 (Figure 1D). RNase R can degrade linear RNA but is unable to degrade circRNA. Through RT-qPCR, we found that RNase R-treated RNA from NOZ cells could not amplify linear EZH2, while the expression of circEZH2 remained unaffected. CircRNAs lack a poly(A) tail structure, preventing amplification through oligo(dT). Our RT-qPCR results indicated that circEZH2 cannot be reverse transcribed solely using oligo(dT) as a primer, whereas this process is different from that used for linear EZH2 (Figures 1E and 1F). These findings verify the circular nature of circEZH2. The subcellular localization of circRNAs provides insight into their functional mechanisms. To elucidate the subcellular localization of circEZH2, we employed fluorescence *in situ* hybridization (FISH), which revealed that circEZH2 was predominantly localized in the cytoplasm of GBC cells (Figure 1G).

circEZH2 promotes GBC progression *in vitro* and *in vivo*

To elucidate the biological function of circEZH2 in GBC, we selected two cell lines, NOZ and SGC-996, which have high expression levels of circEZH2, and used small interfering RNA (siRNA) targeting-specific junction sites to knockdown the expression of circEZH2 (Figure 2A). CCK-8 and EdU cell proliferation assays indicated that cell proliferation was markedly inhibited in the knockdown groups compared to the negative control group (siNC) (Figures 2B–2D). Colony formation assays revealed a decrease in the number of colonies formed by circEZH2 knockdown cells compared to that observed in the control group of NOZ and SGC-996 cells (Figures 2E and 2F). Additionally, flow cytometry was used to assess the impact of circEZH2 on the cell cycle of GBC cells. The results revealed a significant increase in the proportion of G1-phase cells and a significant decrease in the proportion of S-phase cells after circEZH2 knockdown, indicating G1/S cell-cycle arrest in NOZ and SGC-996 cells (Figure 2G). These results indicate that circEZH2 promotes GBC progression *in vitro*.

To further elucidate the role of circEZH2 in GBC progression, we stably knocked down circEZH2 in NOZ cells using a lentivirus to establish shcircEZH2 cells. These cells and the negative control group (shNC) cells were separately injected subcutaneously into two groups of BALB/c nude mice to establish a subcutaneous xenograft tumor model. We observed that, compared with those in the control group, the tumor volume and weight in the shcircEZH2 group were lower (Figures 2H–2K). Immunohistochemistry was used to evaluate the expression of cyclinD1 and Ki67 in xenograft tumor tissues. The results indicates that the expression of CyclinD1 and Ki67 in shcircEZH2 group were lower than that in shNC group (Figure 2L), which suggested that circEZH2 knockdown inhibits the progression of GBC *in vivo*.
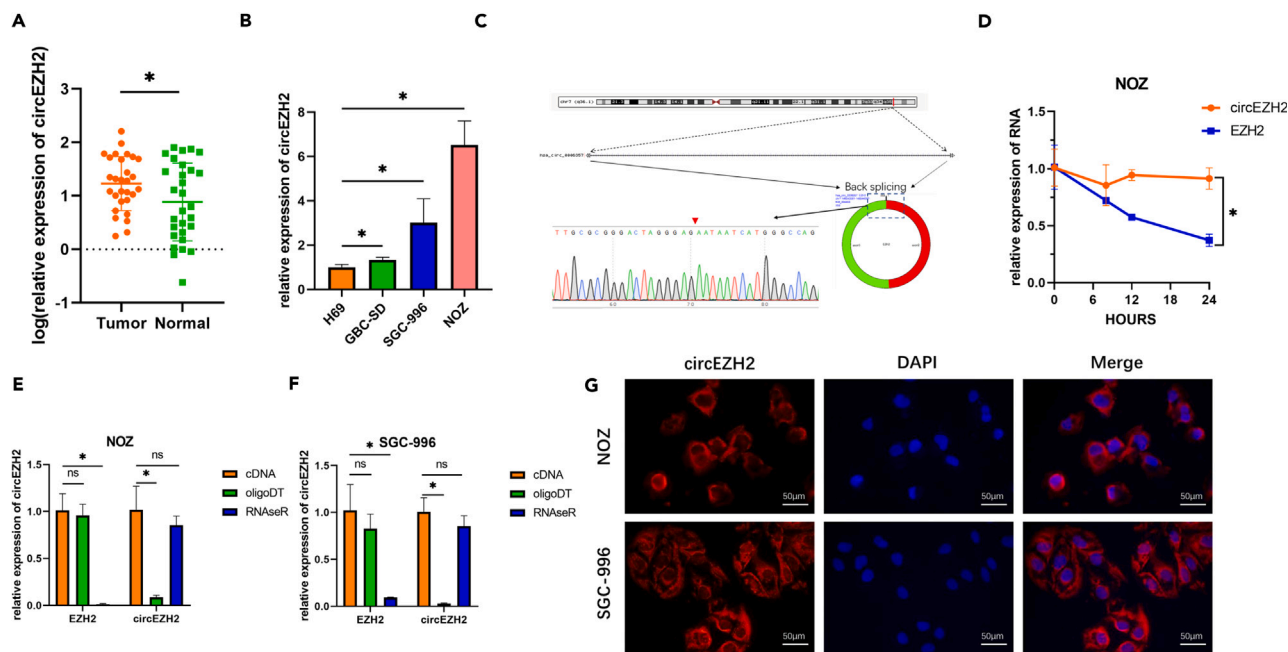
Figure 1. CircEZH2 is upregulated in GBC tissues and cell lines

(A) The RT-qPCR method was applied to detect the expression levels of circEZH2 in 29 GBC tumor tissues and adjacent normal tissues.

(B) The relative expression of circEZH2 in human GBC cell lines and a human normal biliary epithelial cells (H69) by RT-qPCR.

(C) The junction site of circEZH2 was confirmed by amplification with divergent primers and subsequent detection through Sanger sequencing.

(D) RT-qPCR analysis for RNA stabilization of circEZH2 or EZH2 treated with Actinomycin D (2 μg/mL) at the indicated time point.

(E and F) RT-qPCR analysis of circEZH2 by divergent primers and convergent primers in cDNA from total RNA or RNase R-treated RNA.

(G) Fluorescence *in situ* hybridization (FISH) was performed on circEZH2. Data are shown as mean $\pm$ SD. $*p < 0.05$. ns., not significant.

circEZH2 regulates lipid metabolism and ferroptosis in GBC

Previous studies have suggested that metabolic reprogramming plays a crucial role in the malignant progression of GBC.[14,23] Therefore, we conducted untargeted metabolomic analysis to investigate whether circEZH2 regulates metabolism reprogramming. The results revealed a significant alteration in the downstream metabolic profile following the knockdown of circEZH2 (Figures 3A and 3B). Metabolic pathway analysis of the metabolomic data showed that circEZH2 knockdown primarily altered pathways such as "choline metabolism in cancer," "sphingolipid signaling pathway," "necroptosis," "purine metabolism," "glycerophospholipid metabolism," "pyrimidine metabolism," "neuroactive ligand-receptor interaction," "insulin resistance," "sphingolipid metabolism," "cyclic AMP signaling pathway," "insulin secretion," "pancreatic cancer," "thyroid hormone synthesis," and "ABC transporters" (Figure 3C). Glycerophospholipids are the primary constituents of cell membranes, and alterations in their properties can affect membrane stability, inducing ferroptosis.[27] Thus, we extracted glycerophospholipid data from the metabolomics dataset and generated a heatmap, revealing a significant increase in glycerophospholipid levels containing SFAs and a significant decrease in those containing MUFAs in the circEZH2 knockdown group compared to the control group (Figures 3D and 3E). Therefore, our results suggest that circEZH2 can regulate lipid metabolism reprogramming in GBC, particularly by balancing the dynamics between MUFAs and SFAs, which may promote ferroptosis.

Thus, using the BODIPY581/591 fluorescent probe, we investigated whether knocking down circEZH2 affects ferroptosis in GBC cells. We observed a remarkable increase in the fluorescence intensity in the circEZH2 knockdown group compared to that in the control group (Figure 3F), indicating that circEZH2 knockdown promotes ferroptosis in NOZ and SGC-996 cells. GPX4, SLC7A11, ACSL1, ACSL4, LPCAT3, PTGS2, CHAC1, HMOX1, and NRF2 are markers of ferroptosis.[28,29] We observed that the ferroptosis suppressors GPX4 and NRF2 were downregulated, while the ferroptosis inducers ACSL1, ACSL4, LPCAT3, PTGS2, HMOX1, and CHAC1 were upregulated in the circEZH2 knockdown group (Figure 3G). Moreover, we examined the protein levels of GPX4 and NRF2 and found significant decreases in GPX4 and NRF2 protein expression in the circEZH2 knockdown group (Figures 3H–3J). Besides, GPX4 was upregulated in GBC tumor tissues compared to that in adjacent normal tissues (Figure 3K). These results further support the conclusion that circEZH2 regulates ferroptosis in GBC.

CircEZH2 acts as a sponge for miR-556-5p in GBC

circRNA regulates tumor progression through various mechanisms, including acting as a competitive endogenous RNA (ceRNA) to modulate microRNA (miRNA) expression[13] and binding to transcription factors to either promote or inhibit the transcription of downstream genes.[9] The subcellular localization of circRNAs is instrumental in elucidating their specific mechanisms; circRNAs located in the cytoplasm often function as ceRNAs to regulate downstream gene expression. Our research revealed that circEZH2 is primarily distributed in the cytoplasm (Figure 1G).

Table 1. Correlation between clinicopathological characteristics and circEZH2 expression in 29 cases of GBC patients

Clinicopathological characteristics	The number of patients	CircEZH2 expression		p value
		Lower (n = 15)	Higher (n = 14)	
Age				
< 60	17	10	7	0.462
≥60	12	5	7	
Gender				
Male	7	3	4	0.682
Female	22	12	10	
Tumor size				
≤5cm	17	8	9	0.710
> 5cm	12	7	5	
TNM stage				
I-II	13	10	3	0.025*
III-IV	16	5	11	
Lymph node metastasis				
Negative	12	5	7	0.462
Positive	17	10	7	
Histological grade				
Well and moderately	18	8	10	0.450
Poorly and others	11	7	4	
Adjacent organ invasion				
No	14	6	8	0.466
Yes	15	9	6	

*$p < 0.05$. TNM, tumor-node-metastasis.

Therefore, we hypothesize that circEZH2 may regulate downstream gene expression through a ceRNA mechanism. Subsequently, we predicted miRNAs that could interact with circEZH2 using the starBase (https://rnasysu.com/encori/index.php), CircBank (http://www.circbank.cn/), and CircInteractome (https://circinteractome.irp.nia.nih.gov/) databases. By taking the intersection, we identified two candidate miRNAs: miR-556-5p and miR-495-3p (Figure 4A). Through RT-qPCR, we found that knocking down circEZH2 in NOZ cells led to increased expression of both miRNAs, with a more significant increase in miR-556-5p (Figure 4B). To confirm the interaction between circRNAs and miRNAs, we performed RNA pull-down experiments using a biotin-labeled circEZH2 probe. Compared to the negative control probe, the circEZH2 probe significantly enriched miR-556-5p, while miR-495-3p did not exhibit a similar effect (Figure 4C). Conversely, using a biotin-labeled miR-556-5p probe to pull down circEZH2, we observed that the miR-556-5p probe could more effectively pull down circEZH2 than the control probe could (Figure 4D). Both these experiments suggested that circEZH2 can directly or indirectly interact with miR-556-5p. Furthermore, we explored the binding sites between miR-556-5p and circEZH2 by constructing plasmids with mutated binding sites (circEZH2-MUT) and wild-type plasmids (circEZH2-WT) (Figure 4E) and co-transfected them with miR-NC or miR-556-5p mimics into NOZ and SGC-996 cells. We found that, in the circEZH2-WT group, transfection with miR-556-5p mimics significantly decreased the fluorescence intensity compared to that in the control group. However, in the circEZH2-MUT group, there was no significant change in the expression of the target gene, indicating that the mutated site is the binding site between circEZH2 and miR-556-5p (Figures 4F and 4G). These results suggest that miR-556-5p is a direct target of circEZH2.

Subsequently, we verified whether circEZH2 regulates the ferroptosis and proliferation of GBC cells through miR-556-5p. Using the BODIPY581/591 lipid peroxidation fluorescence probe, we found that the induction of ferroptosis by circEZH2 knockdown in NOZ and SGC-996 cells could be partially attenuated by the miR-556-5p inhibitor (Figure 4H). Similarly, in colony formation and CCK-8 experiments, we observed that the inhibition of proliferation caused by circEZH2 knockdown could be partially attenuated by miR-556-5p inhibitor (Figures 4I–4K). These results suggest that circEZH2 may influence ferroptosis and cell proliferation in GBC by regulating the expression of miR-556-5p.

CircEZH2 regulates SCD1 expression by interacting with miR-556-5p in GBC cells

To investigate how circEZH2 regulates ferroptosis in GBC cells through downstream genes, we integrated data from the starBase (https://rnasysu.com/encori/index.php), miRWalk (http://mirwalk.umm.uni-heidelberg.de/), and TargetScan (https://www.targetscan.org/vert_80/)
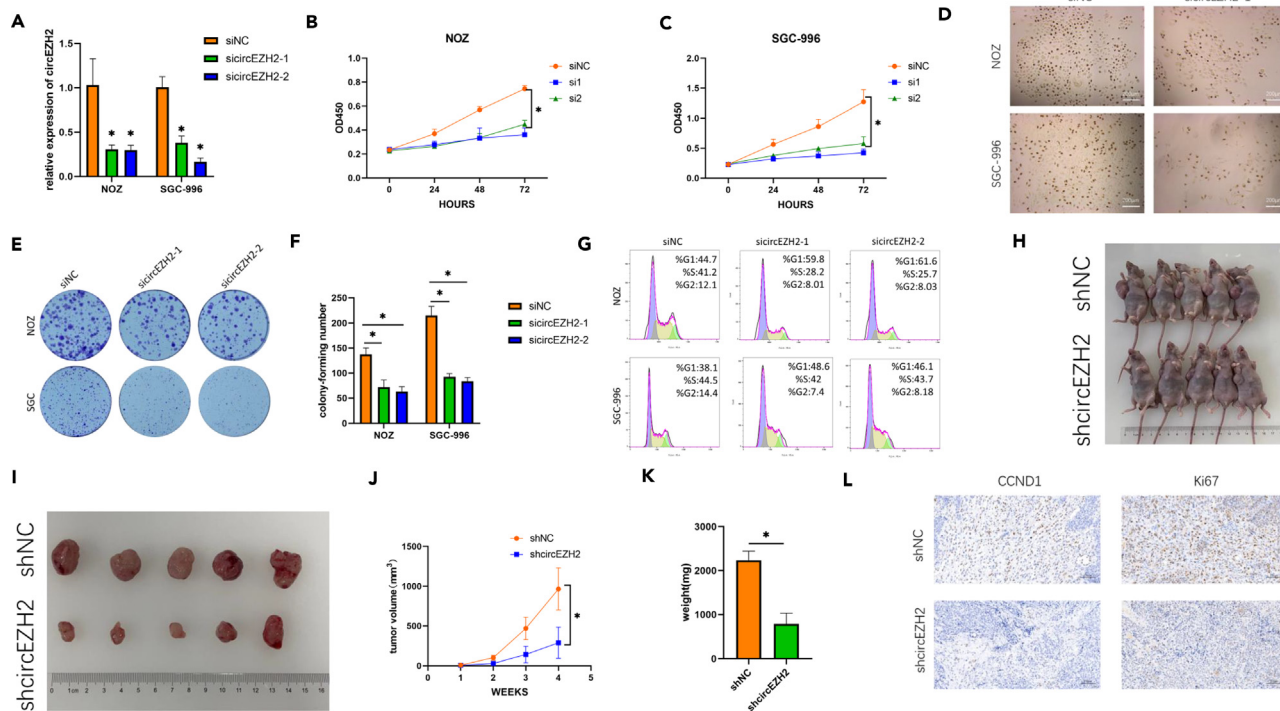
Figure 2. circEZH2 promotes GBC progression *in vitro* and *in vivo*

(A) The relative expression of circEZH2 was detected in NOZ and SGC-996 cells by RT-qPCR analysis after cells were transfected with siNC, sicircEZH2-1, or sicircEZH2-2.

(B and C) CCK-8 assay for cell proliferation capacity after cells were transfected with siRNA at 0–3 days.

(D) 5-Ethynyl-2′-deoxyuridine (EdU) proliferation assay. Knockdown of circEZH2 inhibits DNA synthesis in NOZ and SGC-996 cells. The original magnification was 200×.

(E and F) Colony formation assay was conducted to verify the impact of knockdown circEZH2.

(G) The percentage cell-cycle phase distribution was analyzed by flow cytometry after NOZ and SGC-996 cells were transfected with siNC, sicircEZH2-1, or sicircEZH2-2.

(H–K) The volume and weight of subcutaneous xenograft tumors (*n* = 5 mice per group).

(L) The expression of Ki67 and cyclinD1 by IHC staining. Data are shown as mean $\pm$ SD. *$p < 0.05$.

databases, as well as the ferroptosis suppressor catalog in the FerrDb (http://www.zhounan.org/ferrdb/current/) database. This intersection yielded nine mRNAs: SCD1, LAMP2, CDKN1A, VDR, PRKAA2, AR, TFAM, CREB5, and PPARA (Figure 5A). SCD1 is a member of the stearoyl-CoA desaturase family and has been demonstrated to promote the transformation of SFAs to MUFAs and inhibit ferroptosis in various tumors,[26,30] which is consistent with the effect of circEZH2 knockdown. In addition, SCD1 was upregulated in GBC tumor tissues compared to that in adjacent normal tissues (Figure 5B). Therefore, we hypothesized that circEZH2/miR-556-5p promotes lipid metabolism reprogramming and inhibits ferroptosis in GBC cells by regulating the expression of SCD1. To substantiate this hypothesis, we knocked down circEZH2 in NOZ cells and performed western blotting to evaluate the expression of the SCD1 protein. We observed a decrease in the expression of the SCD1 protein in circEZH2 knockdown group compared to that of control group (Figure 5C), which was the same as that in xenograft tumor tissues (Figure 5D). Next, rescue experiments using a miR-556-5p inhibitor were performed in the NOZ and SGC-996 cell lines. We observed a significant decrease in SCD1 mRNA in both the cell lines with circEZH2 knockdown, which was restored in the sicircEZH2+miR-556-5p inhibitor group (Figure 5E). Furthermore, at the protein level, we found that circEZH2 knockdown in NOZ cells markedly reduced the protein expression level of SCD1, and rescue with the miR-556-5p inhibitor after circEZH2 knockdown restored SCD1 protein expression in both NOZ and SGC-996 cells (Figure 5F). These results suggest that circEZH2/miR-556-5p regulates the expression of SCD1. Furthermore, we elucidated the binding sites between miR-556-5p and SCD1 mRNA. By predicting SCD1 binding sites via the TargetScan database (Figure 5G), we constructed plasmids with mutated SCD1 binding sites (SCD1-MUT) and WT plasmids (SCD1-WT) for dual-luciferase experiments. We found that, in the SCD1-WT group, miR-556-5p mimics significantly decreased the fluorescence intensity, while, in the SCD1-MUT group, the fluorescence intensity did not significantly change (Figures 5H and 5I). These findings suggested that miR-556-5p binds to SCD1 mRNA at this site. In summary, circEZH2 regulates SCD1 expression by interacting with miR-556-5p in GBC cells.
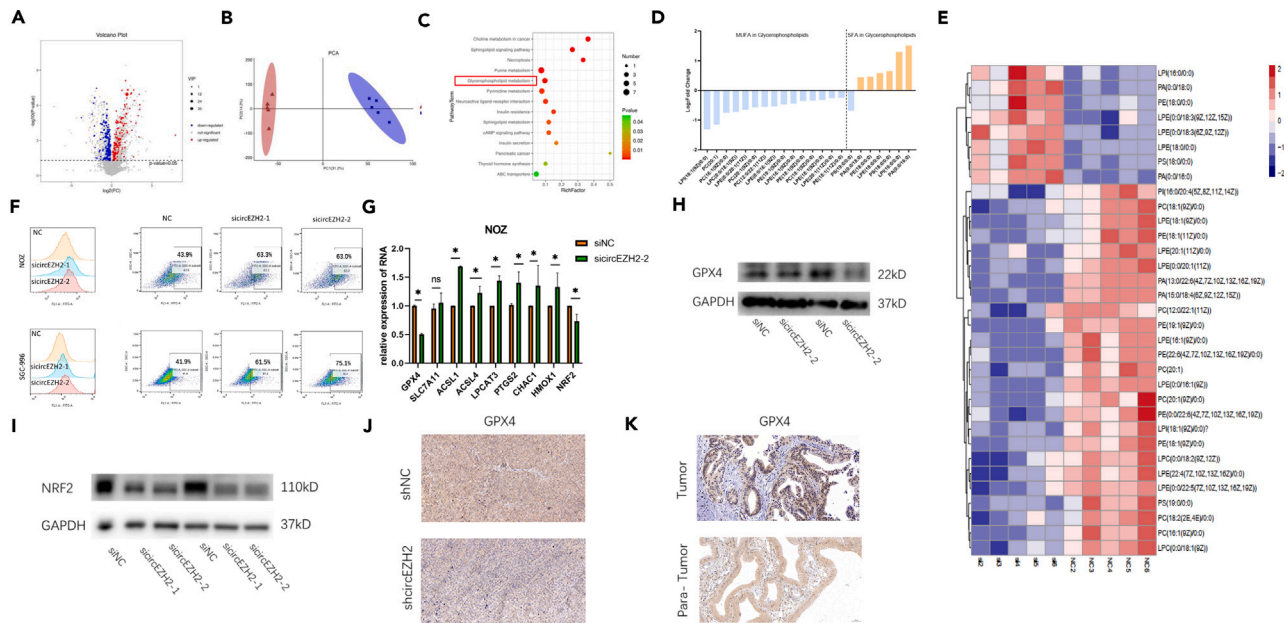
Figure 3. circEZH2 regulates lipid metabolism and ferroptosis in GBC

(A and B) NOZ cells were transfected with siNC or sicircEZH2-2 for volcano plot of the differential metabolite analysis and metabolite principal-component analysis (PCA).

(C) Metabolite pathway analysis after NOZ were transfected with siNC or sicircEZH2-2.

(D and E) Glycerophospholipids contain SFA upregulated while Glycerophospholipids contain MUFA downregulated in NOZ cells after circEZH2 knockdown.

(F) Flow cytometry was applied to detect lipid peroxidation level in NOZ and SGC-996 cells after incubated with a BODIPY C11 probe for 30 min.

(G) The RT-qPCR method was applied to detect the mRNA levels of GPX4, SLC7A11, ACSL1, ACSL4, LPCAT3, PTGS2, CHAC1, HMOX1, and NRF2, which were normalized to β-actin.

(H and I) GPX4 and NRF2 protein levels after circEZH2 knockdown in NOZ cells were detected by western blot.

(J and K) GPX4 protein level in xenograft tumors tissue and GBC patients' tumor or normal tissues were detected by immunohistochemistry. Data are shown as mean ± SD. *$p < 0.05$. ns., not significant. MUFA, monounsaturated fatty acids; SFA, saturated fatty acids; LPC, lysophosphatidylcholines; LPE, lysophosphatidylethanolamines; PC, phosphatidylcholines; PE, phosphatidylethanolamines; PI, phosphatidylinositols; PS, phosphatidylserines.

The IGF2BP2-circEZH2 positive feedback loop upregulates the expression of circEZH2

The following section will explore why circEZH2 is highly expressed in GBC. Previous studies have suggested that some RNA-binding proteins (RBPs) can bind to circRNAs, altering their subcellular localization and expression levels.[31,32] Therefore, we considered the possibility that RBPs bind to circEZH2 to regulate its expression. We conducted RNA pull-down experiments in NOZ cell lines and subjected the pulled-down proteins to SDS-PAGE, followed by silver staining. We observed significant enrichment of proteins at the 55–70 kDa position in the biotin-circEZH2 probe compared to the negative control probe (Figure 6A). To further identify the proteins involved in the pull-down process, we subjected the proteins to liquid chromatography-tandem mass spectrometry (LC-MS/MS), and the results revealed the presence of the RBP IGF2BP2 in the circEZH2-probe group. These findings were validated by western blot analysis (Figure 6B). Additionally, mass spectrometry and western blot data also indicated the presence of AGO2 in the pull-down protein in the circEZH2-probe group (Figure 6B), further confirming the existence of a ceRNA regulatory mechanism involving circEZH2. Subsequently, we performed RBP immunoprecipitation (RIP) experiments using an antibody against IGF2BP2 to validate the interaction between circEZH2 and IGF2BP2. We found that, compared to the amount of circEZH2 enriched by the IgG antibody, the amount of circEZH2 enriched by the IGF2BP2 antibody was significantly increased (Figure 6C). This finding provides reverse validation of the mutual interaction between IGF2BP2 and circEZH2.

IGF2BP2 is an m6A reader protein, and published reports suggest that it can recognize m6A-modified RNA, enhancing its stability.[33,34] We observed that the expression of IGF2BP2 was upregulated in tumor tissue from GBC patients compared to that in para-tumor tissue (Figure 6D). To investigate whether circEZH2 is regulated by IGF2BP2 through m6A modification, we knocked down IGF2BP2 to evaluate the expression of circEZH2. As expected, the expression of circEZH2 was downregulated in the IGF2BP2 knockdown group (Figure 6E). Subsequently, RNA stability experiments were conducted. We found that, over time, the siIGF2BP2 group exhibited a faster decrease in the expression of circEZH2 than the control group. These findings suggested that knocking down IGF2BP2 leads to decrease stability of circEZH2 in GBC cells (Figure 6F). The presence of m6A modification sites in RNA sequences is a prerequisite for RNA m6A modification. Therefore, we analyzed whether circEZH2 has m6A modification sites via the SRAMP website (http://www.cuilab.cn/sramp). Through prediction, an m6A site at position 245 of the circRNA with high confidence was found (Figure 6G). Furthermore, we conducted RIP experiments using a m6A antibody to enrich for circEZH2 and observed a significant increase in circEZH2 enrichment in the m6A antibody-treated group compared
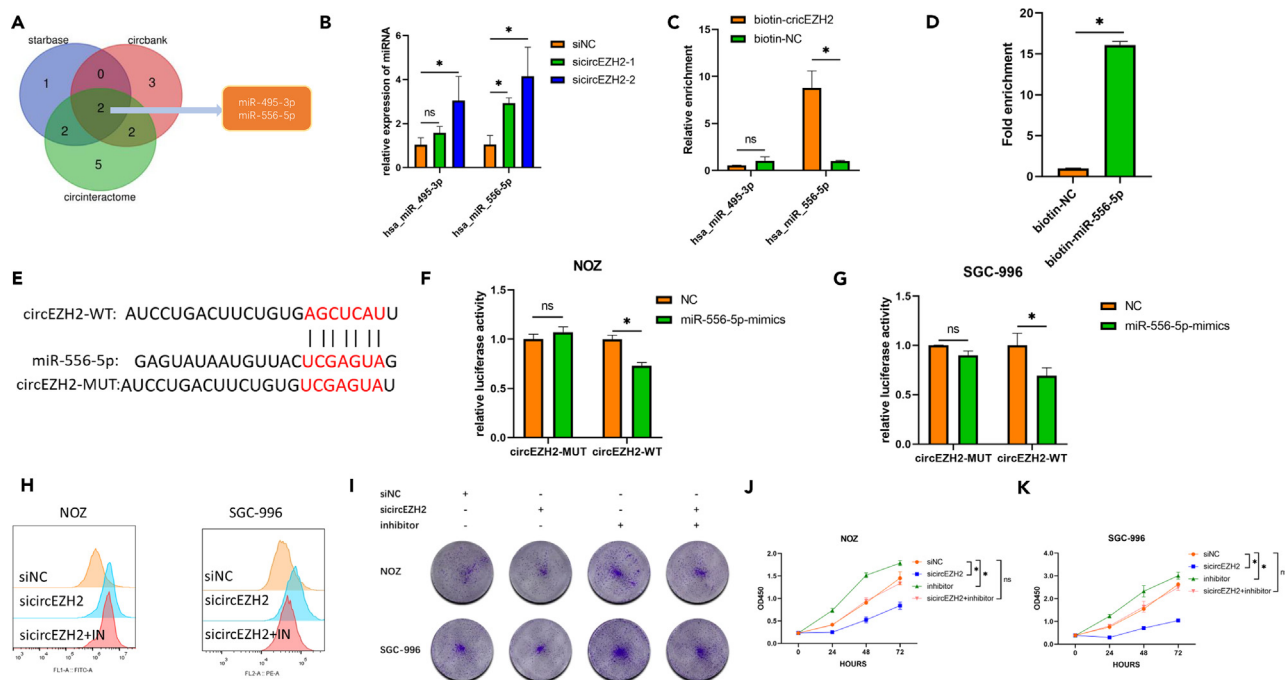
Figure 4. CircEZH2 acts as a sponge for miR-556-5p in GBC

(A) Intersections among three circRNA target prediction algorithms (starBase, circBank, CircInteractome).

(B) The relative expression of miR-556-5p and miR-495-3p was detected after NOZ cells were transfected with siNC, sicircEZH2-1, or sicircEZH2-2 by RT-qPCR analysis.

(C) The bio-circEZH2 or bio-NC group complex was pulled down from NOZ cell lysate with streptavidin-coated magnetic beads, and the expression of miR-556-5p or miR-495-3p was detected by RT-qPCR.

(D) The bio-miR-556-5p or bio-NC group complex was pulled down from NOZ cell lysate with streptavidin-coated magnetic beads, and the expression of circEZH2 was detected by RT-qPCR.

(E) Schematic of the wild-type (WT) or mutant-type (MUT) circEZH2 luciferase reporter vectors was constructed according to the prediction from CircInteractome.

(F and G) The luciferase activities of the circEZH2-WT or circEZH2-MUT luciferase reporter vector in NOZ or SGC-996 cells transfected with miR-556-5p mimics or miR-NC.

(H) Flow cytometry was applied to detect lipid peroxidation level in NOZ and SGC-996 cells after transfected with siNC, sicircEZH2-2, or co-transfected with sicircEZH2-2+ miR-556-5p inhibitor.

(I–K) CCK-8 and colony formation assay was performed to detect the ability of proliferation after transfected with siNC, sicircEZH2-2, or co-transfected with sicircEZH2-2+ miR-556-5p inhibitor. Data are shown as mean ± SD. *$p < 0.05$. ns., not significant.

to the control group. This finding suggested the presence of m6A modifications on circEZH2 (Figure 6H). In conclusion, we determined that IGF2BP2 regulates the stability of circEZH2 by recognizing the m6A modification on circEZH2.

Previous studies have revealed that circEZH2 regulates the ubiquitination of IGF2BP2 in colorectal cancer, thereby influencing the expression of IGF2BP2.[18] Therefore, we explored whether circEZH2 has a similar effect on GBC. Initially, we knocked down circEZH2 in NOZ cells to examine the mRNA and protein expression of IGF2BP2. At the RNA level, we observed no significant difference in IGF2BP2 expression between the circEZH2 knockdown group and the control group (Figure 6I). However, at the protein level, we found that circEZH2 knockdown significantly inhibited the protein expression of IGF2BP2. On the other hand, overexpression of circEZH2 in GBC-SD cells significantly increased the protein expression of IGF2BP2 (Figure 6J). These findings suggested that circEZH2 regulates IGF2BP2 at the protein level. Next, we treated circEZH2 knockdown NOZ cells with the proteasome inhibitor MG132 and observed that the downregulation of IGF2BP2 was reversed after MG132 treatment (Figure 6K). Furthermore, via immunoprecipitation with an anti-IGF2BP2 antibody, we examined the regulatory effect of circEZH2 knockdown on IGF2BP2 protein ubiquitination and found a significant increase in the ubiquitination of IGF2BP2 after circEZH2 knockdown (Figure 6L). In conclusion, we discovered that circEZH2 knockdown can regulate the ubiquitination of IGF2BP2, thereby controlling its protein stability. Taken together, these findings reveal a positive feedback regulatory mechanism between circEZH2 and IGF2BP2 that jointly promotes the upregulation of circEZH2 expression in GBC cells.

In summary, these results demonstrated that circEZH2 is upregulated by the IGF2BP2-circEZH2 positive feedback loop and promotes lipid metabolism reprogramming and the progression of GBC via the circEZH2/miR-556-5p/SCD1 axis.
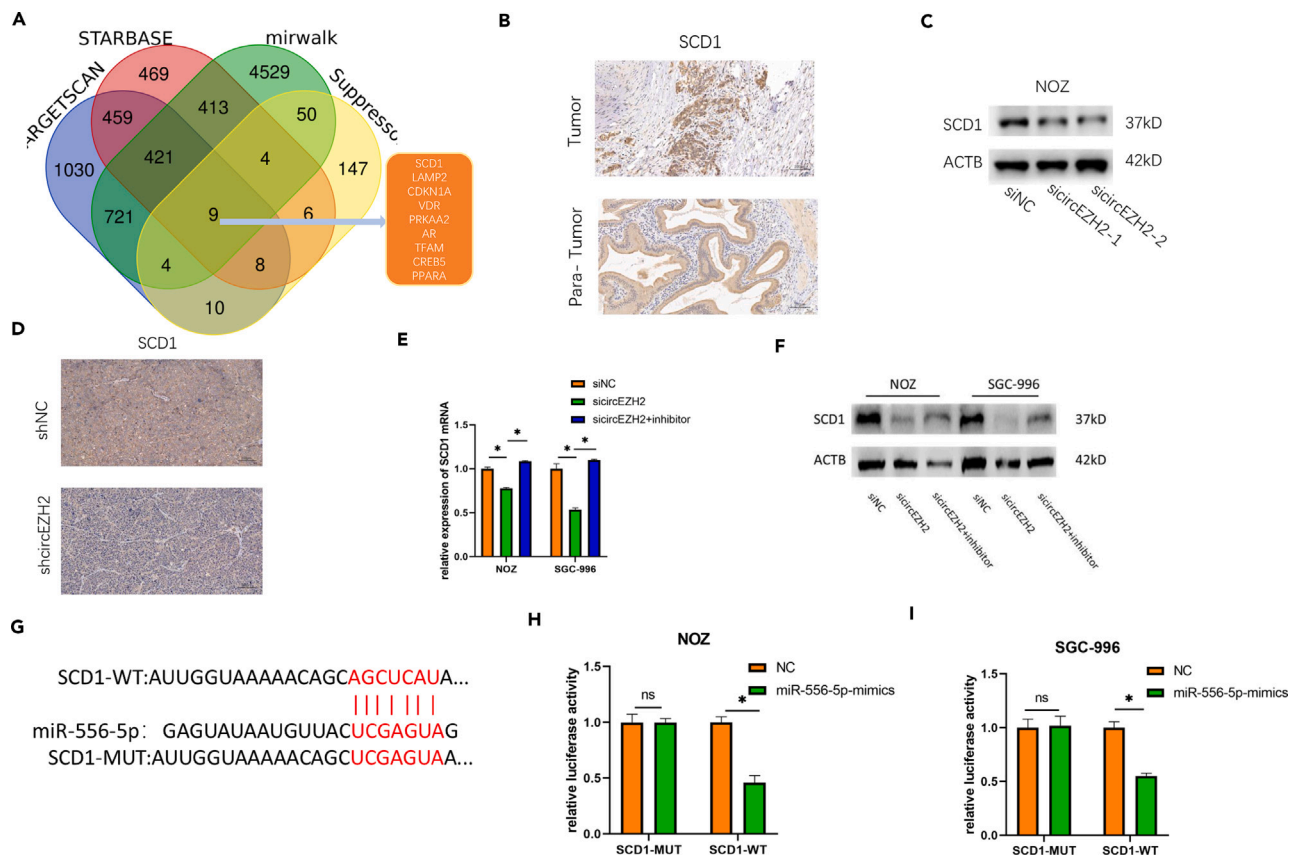
Figure 5. CircEZH2 regulates SCD1 expression by interacting with miR-556-5p in GBC cells

(A) Intersections among three miRNA target prediction algorithms (starBase, TargetScan, miRWalk) and a ferroptosis suppressor catalog in the FerrDb database.

(B) Immunohistochemical staining was shown for SCD1 expression in GBC tumor tissues compared with adjacent normal tissues.

(C) The protein expression of SCD1 was shown by western blot in NOZ cells after cells were transfected with siNC, sicircEZH2-1, and sicircEZH2-2.

(D) SCD1 protein level in xenograft tumors tissue was detected by immunohistochemistry.

(E and F) The mRNA or protein expression of SCD1 was shown by RT-qPCR or western blot in NOZ and SGC-996 cells after cells were transfected with siNC, sicircEZH2-2, or co-transfected with sicircEZH2-2+ miR-556-5p inhibitor.

(G) The WT and corresponding MUT of the SCD1 mRNA 3′ UTR were constructed targeting miR-556-5p.

(H and I) Luciferase reporter assays were performed in NOZ and SGC-996 cells transfected with miR-556-5p mimics, miR-NC and SCD1-WT or SCD1-MUT reporter vector. Data are shown as mean ± SD. *$p < 0.05$. ns., not significant.

DISCUSSION

circRNAs are covalently closed circular noncoding RNAs, and their unique circular structure endows them with resistance to degradation. Previously, circRNAs were considered as by-products of gene transcription, but recent studies have revealed the abnormal expression of circRNAs in various cancer, promoting disease progression. However, there is currently limited research on circRNAs in GBC. CircEZH2 is derived from EZH2 transcripts and was first reported in colorectal cancer. Research has revealed that circEZH2 promotes colorectal cancer progression by regulating the miR-133b/IGF2BP2/CREB axis. Another study revealed the functional role of circEZH2 in prostate cancer (upregulation of EZH2 expression). There are no reports concerning the role of circEZH2 in GBC. In the present study, our results first demonstrated that circEZH2 expression was upregulated in GBC cell lines and tissues. Furthermore, our clinical data showed that high circEZH2 expression was associated with advanced TNM stage. Thus, our results first revealed that the expression of circEZH2 could be a biomarker for GBC prognosis.

circRNAs have been implicated in the regulation of various cellular processes, such as proliferation, apoptosis, migration, and ferroptosis.[35] Our further *in vivo* and *in vitro* experiments showed that circEZH2 knockdown resulted in the inhibition of cell proliferation and cell-cycle progression while promoting ferroptosis in GBC cells. These findings suggest that inhibiting circEZH2 could be a targeted therapeutic approach for GBC. Additionally, metabolic reprogramming is a characteristic feature of tumor cells adapting to the unique tumor microenvironment and has become a hallmark of cancer.[36] Lipid metabolism reprogramming is one facet of tumor metabolic reprogramming and has been found to play a crucial role in the progression of various malignancies.[37,38] Previous studies have demonstrated that circRNAs function in regulating lipid metabolism reprogramming, thereby promoting malignant progression.[39] circRIC8B, an upregulated circRNA in chronic lymphocytic leukemia, can reprogram lipid metabolism through the miR-199b-5p/LPL axis.[35] Furthermore, in biliary tract tumors, our previous
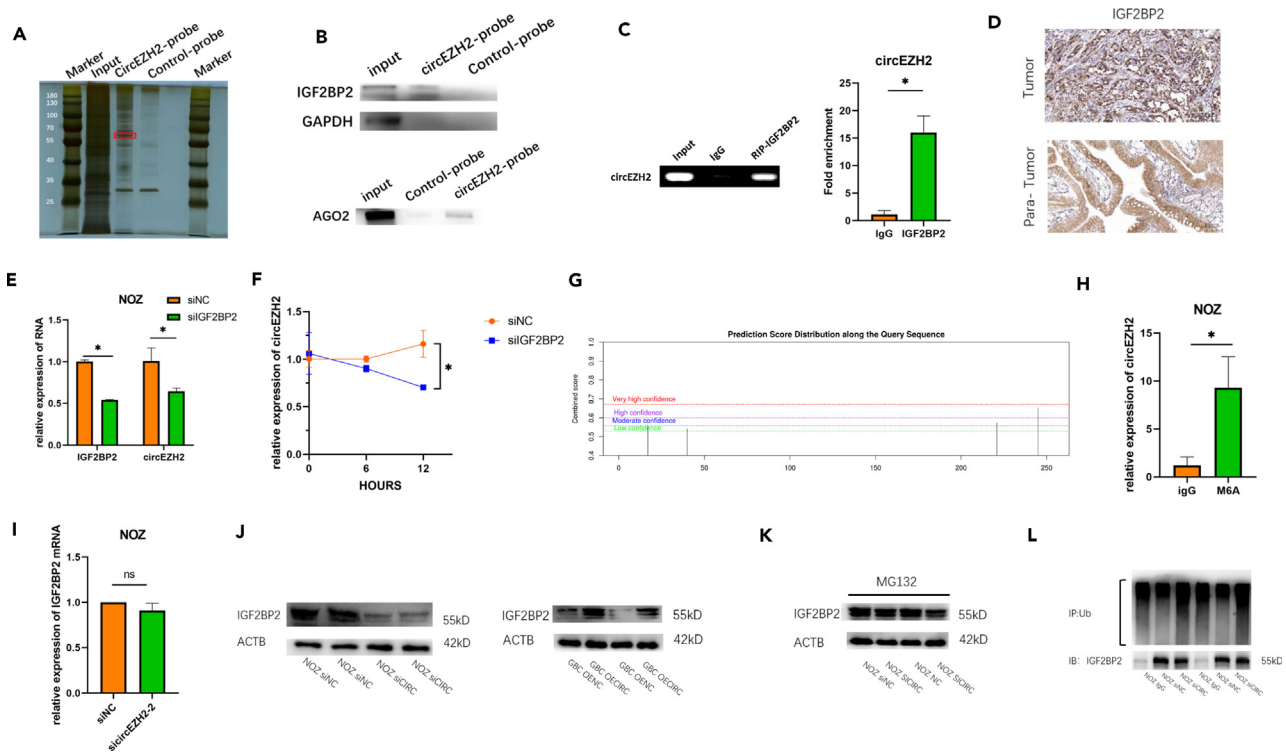
Figure 6. The IGF2BP2-circEZH2 positive feedback loop upregulates the expression of circEZH2

(A) RNA pull-down assay combined with silver staining was used to detect circEZH2-related proteins.

(B) Western blot analysis was performed to verify the interaction of circEZH2 and IGF2BP2 or AGO2. GAPDH was used as a negative control.

(C) RNA immunoprecipitation (RIP) assay was performed to further verify the interaction between circEZH2 and IGF2BP2 in NOZ cells. IgG was used as a negative control.

(D) Immunohistochemical staining was shown for IGF2BP2 expression in GBC tissues compared with adjacent normal tissues.

(E) RT-qPCR was applied to detect the expression of circEZH2 in NOZ cells after transfected with siNC or siIGF2BP2.

(F) RT-qPCR analysis for RNA stabilization of circEZH2 in NOZ cells after transfected with siNC or siIGF2BP2 at the indicated time point.

(G) The m6A modification sites of circEZH2 was predicted from the SRAMP database.

(H) RIP was applied to evaluate the level of m6a modification in circEZH2.

(I and J) RT-qPCR and western blot were used to detect the expression of IGF2BP2 in NOZ or GBC-SD cells after transfected with siNC, sicircEZH2-2, pLCDH-vector, or pLCDH-circEZH2.

(K) CircEZH2 knockdown and control NOZ cells were incubated with MG132 (10 µM) for 8 h. Protein levels of IGF2BP2 were measured by western blot.

(L) Immunoprecipitation detected ubiquitination modification of IGF2BP2 with MG132 treatment in NOZ cells. IgG was used as a negative control. Data are shown as mean $\pm$ SD. *p < 0.05. ns., not significant, Ub, ubiquitin.

research revealed high expression of circMBOAT2 in intrahepatic cholangiocarcinoma. It regulates lipid spectrum changes through the PTBP1/FASN axis, promoting malignant progression.[40] In this study, we found that knockdown of circEZH2 in GBC cells significantly altered the lipid metabolism profile, with the most notable change being an increase in the ratio of glycerophospholipids containing SFAs to those containing MUFAs, which may sensitize tumor cells to ferroptosis. These results suggest that circEZH2 promotes lipid metabolism reprogramming in GBC cells.

Previous studies have indicated that circRNAs play a crucial role in regulating the malignant progression of tumors through various mechanisms. For instance, our prior studies have demonstrated that circRNAs such as circTP63,[15] circPVT1,[17] and circβ-catenin[16] modulate downstream gene expression through ceRNA mechanisms, thereby promoting the malignant progression of GBC. On the other hand, circFOXP1[14] and circMBOAT2[40] facilitate tumor malignancy by regulating the subcellular localization of downstream mRNAs through binding PTBP1. In the present study, we discovered that circEZH2 can interact with AGO2 to execute ceRNA-mediated regulatory mechanisms. These findings align with previous reports of circEZH2 in colorectal cancer and prostate cancer. However, a distinctive aspect of this study is the identification of miR-556-5p, rather than miR-133b, miR-363, or miR-708, as the downstream miRNA for circEZH2.[18,19] This discrepancy may be associated with tumor heterogeneity. Through reciprocal pull-down experiments, we confirmed the mutual interaction between miR-556-5p and circEZH2. Additionally, dual-luciferase assays revealed the binding site of miR-556-5p with circEZH2. Therefore, our findings suggest that circEZH2 promotes the malignant progression of GBC through sponging with miR-556-5p.

SCD1 is a type of desaturase enzyme involved in the production of MUFAs, and it is highly expressed in various tumors. Previous studies have suggested that SCD1 plays a role in dynamically balancing the saturation state of cellular lipids, thereby conferring tolerance to ferroptosis, a form of iron-dependent cell death.[26,30] Our research indicated that SCD1 is a downstream target gene of circEZH2. Mechanistically, we clarified the interaction site between miR-556-5p and SCD1 through dual-luciferase reporter experiments. Furthermore, we observed that the miR-556-5p inhibitor could reverse the ferroptosis and the downregulation of SCD1 induced by circEZH2 knockdown at both the RNA and protein levels. These findings underscore the role of the circEZH2/miR-556-5p/SCD1 axis in regulating the malignant progression of GBC and lipid metabolism reprogramming.

IGF2BP2 is an m6A reader protein, and studies suggest that it can recognize m6A modification sites on RNA, thereby enhancing the stability of the corresponding RNA. SOX2 and circRUNX1 are both regulated by IGF2BP2 to increase RNA stability.[31,34] Our study investigated the mechanism underlying the upregulation of circEZH2 in GBC. Through RNA pull-down combined with mass spectrometry analysis and reciprocal RNA binding protein immunoprecipitation experiments, we demonstrated that circEZH2 can interact with IGF2BP2. Furthermore, we found that circEZH2 undergoes m6A modification, and knockdown of IGF2BP2 leads to decreased the expression and stability of circEZH2. Therefore, we propose that IGF2BP2 can regulate circEZH2 expression through the m6A mechanism. In addition, based on related studies in colorectal cancer, the binding of circEZH2 to IGF2BP2 reduces the ubiquitination and degradation of the latter.[18] To validate this finding in GBC, we knocked down circEZH2 and revealed no significant impact on the mRNA level of IGF2BP2. On the other hand, circEZH2 knockdown significantly decreased the protein level of IGF2BP2. Further immunoprecipitation experiments revealed that circEZH2 knockdown in GBC cells increased the ubiquitination level of IGF2BP2, promoting its degradation. Therefore, we discovered that circEZH2 and IGF2BP2 constitute a positive feedback loop to promote the upregulation of circEZH2 expression.

In conclusion, our results first demonstrated that the IGF2BP2-circEZH2 positive feedback loop upregulates the expression of circEZH2 in GBC, which regulates tumor growth and lipid metabolism reprogramming through miR-556-5p, enhancing its ability to target SCD1. Thus, we propose that circEZH2 could be a potential biological marker and therapeutic target for GBC.

Limitations of the study and future research directions

Our study indicates that the expression of circEZH2 is correlated with the TNM staging of GBC tumors, which may hint that patients with high expression of circEZH2 may have lower OS or progression-free survival (PFS). However, due to the lack of follow-up data in this study, we are unable to assess this. Future research could increase the sample size and combine the expression of circEZH2 with patient follow-up data to evaluate the relationship between the expression of circEZH2 and OS or PFS of GBC patients.

The circEZH2 expression levels assessed in this study were on GBC tissues, which limits the potential clinical application of circEZH2. Therefore, the future study will explore the differences in circEZH2 content between blood samples from GBC patients and normal individuals. Additionally, the current treatment for GBC still relies on systemic chemotherapy based on gemcitabine, but the effectiveness is limited. Whether the expression level of circEZH2 can predict the sensitivity of GBC patients to chemotherapy will be clarified in future research.

Our study has demonstrated that the m6A modification of IGF2BP2 enhances the stability of circEZH2, thereby increasing its expression level. However, the specific modification sites and mechanism have not yet been identified, and further research is needed to explore this. As previously mentioned, circRNAs have various regulatory mechanisms to control the expression of downstream genes. Our research has found that circEZH2 can regulate the expression of SCD1 through the ceRNA mechanism. There may also be other mechanisms at play, such as regulating the transcription and translation of SCD1 by binding to related proteins, which will require further research to explore.

STAR★METHODS

Detailed methods are provided in the online version of this paper and include the following:

- KEY RESOURCES TABLE
- RESOURCE AVAILABILITY
  - Lead contact
  - Materials availability
  - Data and code availability
- EXPERIMENTAL MODEL AND STUDY PARTICIPANT DETAILS
  - Patients tissue samples
  - Cell lines culture
  - Animal experiments
- METHOD DETAILS
  - Cell transfection
  - Cell proliferation, colony formation assay
  - 5-Ethynyl-2′-deoxyuridine (EdU) proliferation assay
  - Cell cycle detection
  - Immunohistochemistry (IHC), Fluorescence *in situ* hybridization (FISH)
  - Actinomycin D assays
  - RNA extraction and RT-qPCR analysis

- ○ RNase R treatment
- ○ Western blotting assays
- ○ LC-MS Untargeted Metabonomics
- ○ miRNA pull down
- ○ RNA pull-down assay, silver staining and mass spectrometry analysis
- ○ Lipid peroxidation detection
- ○ Co-immunoprecipitation
- ○ Luciferase reporter assays
- ○ Ethics approval and consent to participate
- ● QUANTIFICATION AND STATISTICAL ANALYSIS
- ● ADDITIONAL RESOURCES

SUPPLEMENTAL INFORMATION

Supplemental information can be found online at https://doi.org/10.1016/j.isci.2024.110428.

AUTHOR CONTRIBUTIONS

T.Z. and W.S. conceived the project and supervised the project. T.H., Y.X., Z.L., and Z.D. performed the biological experiments. L.B. and Y.J. performed the molecular experiments. S.Z., C.J., and S.Y. collected clinical data. T.H. analyzed the data and wrote the paper. All the authors have read and approved the final paper.

DECLARATION OF INTERESTS

The authors declare no competing interests.

REFERENCES

1. Roa, J.C., García, P., Kapoor, V.K., Maithel, S.K., Javle, M., and Koshiol, J. (2022). Gallbladder cancer. Nat. Rev. Dis. Prim. *8*, 69. https://doi.org/10.1038/s41572-022-00398-y.

2. Feo, C.F., Ginesu, G.C., Fancellu, A., Perra, T., Ninniri, C., Deiana, G., Scanu, A.M., and Porcu, A. (2022). Current management of incidental gallbladder cancer: A review. Int. J. Surg. *98*, 106234. https://doi.org/10.1016/j.ijsu.2022.106234.

3. Sung, H., Ferlay, J., Siegel, R.L., Laversanne, M., Soerjomataram, I., Jemal, A., and Bray, F. (2021). Global Cancer Statistics 2020: GLOBOCAN Estimates of Incidence and Mortality Worldwide for 36 Cancers in 185 Countries. CA A Cancer J. Clin. *71*, 209–249. https://doi.org/10.3322/caac.21660.

4. D'Hondt, M., Lapointe, R., Benamira, Z., Pottel, H., Plasse, M., Letourneau, R., Roy, A., Dagenais, M., and Vandenbroucke-Menu, F. (2013). Carcinoma of the gallbladder: patterns of presentation, prognostic factors and survival rate. An 11-year single centre experience. Eur. J. Surg. Oncol. *39*, 548–553. https://doi.org/10.1016/j.ejso.2013.02.010.

5. Sahu, S., and Sun, W. (2017). Targeted therapy in biliary tract cancers-current limitations and potentials in the future. J. Gastrointest. Oncol. *8*, 324–336. https://doi.org/10.21037/jgo.2016.09.16.

6. Chen, L.L., and Yang, L. (2015). Regulation of circRNA biogenesis. RNA Biol. *12*, 381–388. https://doi.org/10.1080/15476286.2015.1020271.

7. Li, J., Xu, Q., Huang, Z.J., Mao, N., Lin, Z.T., Cheng, L., Sun, B., and Wang, G. (2021). CircRNAs: a new target for the diagnosis and treatment of digestive system neoplasms. Cell Death Dis. *12*, 205. https://doi.org/10.1038/s41419-021-03495-0.

8. Gao, X., Xia, X., Li, F., Zhang, M., Zhou, H., Wu, X., Zhong, J., Zhao, Z., Zhao, K., Liu, D., et al. (2021). Circular RNA-encoded oncogenic E-cadherin variant promotes glioblastoma tumorigenicity through activation of EGFR-STAT3 signalling. Nat. Cell Biol. *23*, 278–291. https://doi.org/10.1038/s41556-021-00639-4.

9. Chen, Q., Wang, H., Li, Z., Li, F., Liang, L., Zou, Y., Shen, H., Li, J., Xia, Y., Cheng, Z., et al. (2022). Circular RNA ACTN4 promotes intrahepatic cholangiocarcinoma progression by recruiting YBX1 to initiate FZD7 transcription. J. Hepatol. *76*, 135–147. https://doi.org/10.1016/j.jhep.2021.08.027.

10. Kristensen, L.S., Hansen, T.B., Venø, M.T., and Kjems, J. (2018). Circular RNAs in cancer: opportunities and challenges in the field. Oncogene *37*, 555–565. https://doi.org/10.1038/onc.2017.361.

11. Shen, Y., Zhang, N., Chai, J., Wang, T., Ma, C., Han, L., and Yang, M. (2023). CircPDIA4 Induces Gastric Cancer Progression by Promoting ERK1/2 Activation and Enhancing Biogenesis of Oncogenic circRNAs. Cancer Res. *83*, 538–552. https://doi.org/10.1158/0008-5472.Can-22-1923.

12. Sang, Y., Chen, B., Song, X., Li, Y., Liang, Y., Han, D., Zhang, N., Zhang, H., Liu, Y., Chen, T., et al. (2019). circRNA_0025202 Regulates Tamoxifen Sensitivity and Tumor Progression via Regulating the miR-182-5p/FOXO3a Axis in Breast Cancer. Mol. Ther. *27*, 1638–1652. https://doi.org/10.1016/j.ymthe.2019.05.011.

13. Yao, B., Zhu, S., Wei, X., Chen, M.K., Feng, Y., Li, Z., Xu, X., Zhang, Y., Wang, Y., Zhou, J., et al. (2022). The circSPON2/miR-331-3p axis regulates PRMT5, an epigenetic regulator of CAMK2N1 transcription and prostate cancer progression. Mol. Cancer *21*, 119. https://doi.org/10.1186/s12943-022-01598-6.

14. Wang, S., Zhang, Y., Cai, Q., Ma, M., Jin, L.Y., Weng, M., Zhou, D., Tang, Z., Wang, J.D., and Quan, Z. (2019). Circular RNA FOXP1 promotes tumor progression and Warburg effect in gallbladder cancer by regulating

PKLR expression. Mol. Cancer *18*, 145. https://doi.org/10.1186/s12943-019-1078-z.

15. Wang, S., Tong, H., Su, T., Zhou, D., Shi, W., Tang, Z., and Quan, Z. (2021). CircTP63 promotes cell proliferation and invasion by regulating EZH2 via sponging miR-217 in gallbladder cancer. Cancer Cell Int. *21*, 608–619. https://doi.org/10.1186/s12935-021-02316-w.

16. Wang, S., Su, T., Tong, H., Zhou, D., Ma, F., Ding, J., Hao, Y., Shi, W., and Quan, Z. (2021). Circβ-catenin promotes tumor growth and Warburg effect of gallbladder cancer by regulating STMN1 expression. Cell Death Dis. *7*, 233–244. https://doi.org/10.1038/s41420-021-00626-6.

17. Wang, S., Su, T.T., Tong, H., Shi, W., Ma, F., and Quan, Z. (2021). CircPVT1 promotes gallbladder cancer growth by sponging miR-339-3p and regulates MCL-1 expression. Cell Death Dis. *7*, 191–199. https://doi.org/10.1038/s41420-021-00577-y.

18. Yao, B., Zhang, Q., Yang, Z., An, F., Nie, H., Wang, H., Yang, C., Sun, J., Chen, K., Zhou, J., et al. (2022). CircEZH2/miR-133b/IGF2BP2 aggravates colorectal cancer progression via enhancing the stability of m(6)A-modified CREB1 mRNA. Mol. Cancer *21*, 140. https://doi.org/10.1186/s12943-022-01608-7.

19. Su, Z., Zhang, M., Luo, H., Zhong, J., Tan, J., Xu, Y., Pan, X., Zeng, H., Nie, L., Xu, M., et al. (2023). circEZH2(E2) (/E3) is a dual suppressor of miR363/miR708 to promote EZH2 expression and prostate cancer progression. Cancer Sci. *114*, 1378–1395. https://doi.org/10.1111/cas.15694.

20. Pavlova, N.N., Zhu, J., and Thompson, C.B. (2022). The hallmarks of cancer metabolism: Still emerging. Cell Metabol. *34*, 355–377. https://doi.org/10.1016/j.cmet.2022.01.007.

21. Zuo, M., Rashid, A., Wang, Y., Jain, A., Li, D., Behari, A., Kapoor, V.K., Koay, E.J., Chang, P., Vauthey, J.N., et al. (2016). RNA sequencing-based analysis of gallbladder cancer reveals the importance of the liver X receptor and lipid metabolism in gallbladder cancer. Oncotarget *7*, 35302–35312. https://doi.org/10.18632/oncotarget.9181.

22. Liu, L., Li, Y., Cao, D., Qiu, S., Li, Y., Jiang, C., Bian, R., Yang, Y., Li, L., Li, X., et al. (2021). SIRT3 inhibits gallbladder cancer by induction of AKT-dependent ferroptosis and blockade of epithelial-mesenchymal transition. Cancer Lett. *510*, 93–104. https://doi.org/10.1016/j.canlet.2021.04.007.

23. Cheng, H., Sun, Y., Yu, X., Zhou, D., Ding, J., Wang, S., and Ma, F. (2023). FASN promotes gallbladder cancer progression and reduces cancer cell sensitivity to gemcitabine through PI3K/AKT signaling. Drug Discov. Ther. *17*, 328–339. https://doi.org/10.5582/ddt.2023.01036.

24. Chen, H., Qi, Q., Wu, N., Wang, Y., Feng, Q., Jin, R., and Jiang, L. (2022). Aspirin promotes RSL3-induced ferroptosis by suppressing mTOR/SREBP-1/SCD1-mediated lipogenesis in PIK3CA-mutant colorectal cancer. Redox Biol. *55*, 102426. https://doi.org/10.1016/j.redox.2022.102426.

25. Luis, G., Godfroid, A., Nishiumi, S., Cimino, J., Blacher, S., Maquoi, E., Wery, C., Collignon, A., Longuespée, R., Montero-Ruiz, L., et al. (2021). Tumor resistance to ferroptosis driven by Stearoyl-CoA Desaturase-1 (SCD1) in cancer cells and Fatty Acid Biding Protein-4 (FABP4) in tumor microenvironment promote tumor recurrence. Redox Biol. *43*, 102006. https://doi.org/10.1016/j.redox.2021.102006.

26. Xuan, Y., Wang, H., Yung, M.M., Chen, F., Chan, W.S., Chan, Y.S., Tsui, S.K., Ngan, H.Y., Chan, K.K., and Chan, D.W. (2022). SCD1/FADS2 fatty acid desaturases equipoise lipid metabolic activity and redox-driven ferroptosis in ascites-derived ovarian cancer cells. Theranostics *12*, 3534–3552. https://doi.org/10.7150/thno.70194.

27. Melero, A., and Jiménez-Rojo, N. (2023). Cracking the membrane lipid code. Curr. Opin. Cell Biol. *83*, 102203. https://doi.org/10.1016/j.ceb.2023.102203.

28. Bersuker, K., Hendricks, J.M., Li, Z., Magtanong, L., Ford, B., Tang, P.H., Roberts, M.A., Tong, B., Maimone, T.J., Zoncu, R., et al. (2019). The CoQ oxidoreductase FSP1 acts parallel to GPX4 to inhibit ferroptosis. Nature *575*, 688–692. https://doi.org/10.1038/s41586-019-1705-2.

29. Dodson, M., Castro-Portuguez, R., and Zhang, D.D. (2019). NRF2 plays a critical role in mitigating lipid peroxidation and ferroptosis. Redox Biol. *23*, 101107. https://doi.org/10.1016/j.redox.2019.101107.

30. Ascenzi, F., De Vitis, C., Maugeri-Saccà, M., Napoli, C., Ciliberto, G., and Mancini, R. (2021). SCD1, autophagy and cancer: implications for therapy. J. Exp. Clin. Cancer Res. *40*, 265. https://doi.org/10.1186/s13046-021-02067-6.

31. Wang, C., Zhou, M., Zhu, P., Ju, C., Sheng, J., Du, D., Wan, J., Yin, H., Xing, Y., Li, H., et al. (2022). IGF2BP2-induced circRUNX1 facilitates the growth and metastasis of esophageal squamous cell carcinoma through miR-449b-5p/FOXP3 axis. J. Exp. Clin. Cancer Res. *41*, 347. https://doi.org/10.1186/s13046-022-02550-8.

32. Jiang, X., Guo, S., Wang, S., Zhang, Y., Chen, H., Wang, Y., Liu, R., Niu, Y., and Xu, Y. (2022). EIF4A3-Induced circARHGAP29 Promotes Aerobic Glycolysis in Docetaxel-Resistant Prostate Cancer through IGF2BP2/c-Myc/LDHA Signaling. Cancer Res. *82*, 831–845. https://doi.org/10.1158/0008-5472.Can-21-2988.

33. Weng, H., Huang, F., Yu, Z., Chen, Z., Prince, E., Kang, Y., Zhou, K., Li, W., Hu, J., Fu, C., et al. (2022). The m(6)A reader IGF2BP2 regulates glutamine metabolism and represents a therapeutic target in acute myeloid leukemia. Cancer Cell *40*, 1566–1582.e10. https://doi.org/10.1016/j.ccell.2022.10.004.

34. Li, T., Hu, P.S., Zuo, Z., Lin, J.F., Li, X., Wu, Q.N., Chen, Z.H., Zeng, Z.L., Wang, F., Zheng, J., et al. (2019). METTL3 facilitates tumor progression via an m(6)A-IGF2BP2-dependent mechanism in colorectal carcinoma. Mol. Cancer *18*, 112. https://doi.org/10.1186/s12943-019-1038-7.

35. Wu, Z., Gu, D., Wang, R., Zuo, X., Zhu, H., Wang, L., Lu, X., Xia, Y., Qin, S., Zhang, W., et al. (2022). CircRIC8B regulates the lipid metabolism of chronic lymphocytic leukemia through miR199b-5p/LPL axis. Exp. Hematol. Oncol. *11*, 51. https://doi.org/10.1186/s40164-022-00302-0.

36. Hanahan, D. (2022). Hallmarks of Cancer: New Dimensions. Cancer Discov. *12*, 31–46. https://doi.org/10.1158/2159-8290.Cd-21-1059.

37. Li, D., and Li, Y. (2020). The interaction between ferroptosis and lipid metabolism in cancer. Signal Transduct. Targeted Ther. *5*, 108. https://doi.org/10.1038/s41392-020-00216-5.

38. Bian, X., Liu, R., Meng, Y., Xing, D., Xu, D., and Lu, Z. (2021). Lipid metabolism and cancer. J. Exp. Med. *218*, e20201606. https://doi.org/10.1084/jem.20201606.

39. Yang, Y., Luo, D., Shao, Y., Shan, Z., Liu, Q., Weng, J., He, W., Zhang, R., Li, Q., Wang, Z., and Li, X. (2023). circCAPRIN1 interacts with STAT2 to promote tumor progression and lipid synthesis via upregulating ACC1 expression in colorectal cancer. Cancer Commun. *43*, 100–122. https://doi.org/10.1002/cac2.12380.

40. Yu, X., Tong, H., Chen, J., Tang, C., Wang, S., Si, Y., Wang, S., and Tang, Z. (2023). CircRNA MBOAT2 promotes intrahepatic cholangiocarcinoma progression and lipid metabolism reprogramming by stabilizing PTBP1 to facilitate FASN mRNA cytoplasmic export. Cell Death Dis. *14*, 20. https://doi.org/10.1038/s41419-022-05540-y.

STAR★METHODS

KEY RESOURCES TABLE

REAGENT or RESOURCE	SOURCE	IDENTIFIER
Antibodies		
Anti-cyclinD1	Abclonal	Cat# A11022; RRID: AB_2758370
Anti-Ki-67	Cell Signaling Technology	Cat# 9027; RRID: AB_2636984
Anti-GPX4	Proteintech	Cat# 67763-1-Ig; RRID: AB_2909469
Anti-SCD1	ABclonal	Cat# A16429; RRID: AB_2772150
Anti-IGF2BP2	Proteintech	Cat# 11601-1-AP; RRID: AB_2122672
Anti-NRF2	Cell Signaling Technology	Cat# 12721; RRID: AB_2715528
Anti-AGO2	Abcam	Cat# ab186733; RRID: AB_2713978
Anti-GAPDH	Cell Signaling Technology	Cat# 2118; RRID: AB_561053
Anti-ubiquitin	Proteintech	Cat# 80992-1-RR; RRID: AB_2923694
Anti-ACTB	Proteintech	Cat# 60008-2-Ig; RRID: AB_2223182
Anti-IgG	Cell Signaling Technology	Cat# 2729; RRID: AB_1031062
Bacterial and virus strains		
Lentivirus	This paper	N/A
Biological samples		
Human gallbladder cancer tissues and matched adjacent normal tissues	Xinhua Hospital, affiliated with Shanghai Jiao Tong University School of Medicine	N/A
Subcutaneous tumor tissue in nude mice	This paper	N/A
Chemicals, peptides, and recombinant proteins		
DMEM medium	Gibco	C11995500BT
DAPI	Beyotime	C1002
Lipofectamine 3000 Reagent	Invitrogen	L3000015
CCK-8 reagent	Beyotime	C0037
RIPA buffer	Beyotime	P0013C
Propidium Iodide	Beyotime	ST511
Actinomycin D	Sigma	SBR00013
TRIzol reagent	TaKaRa	Takara.9108
PrimeScript™ RT Master Mix (Perfect Real Time)	TaKaRa	RR036A
Hieff UNICON® qPCR SYBR® Green Master Mix	Yeasen	11198ES
Geneseed RNase R	Geneseed	R0301
protease inhibitor cocktail	Yeasen	20123ES10
PVDF membrane	Millipore	ISEQ10100
SDS-PAGE Sample Loading Buffer	Beyotime	P0015
Protein A+G Agarose	Beyotime	P2019
Critical commercial assays		
Pierce Magnetic RNA Protein Pull-Down Kit	Thermo Fisher Scientific	20164
RNA Immunoprecipitation kit	Geneseed	P0101
BeyoClickTM EdU proliferation assay kit	Beyotime	C0085L
Alexa FluorTM 488 Tyramide SuperBoost™ Kit	Thermo Fisher Scientific	B40932
T7 High Yield RNA Transcription Kit	Vazyme	TR101
RNeasy Mini Kit	Qiagen	74134

(Continued on next page)

Continued

REAGENT or RESOURCE	SOURCE	IDENTIFIER
The Pierce™ RNA 3′ End Desthiobiotinylation Kit	Thermo Fisher Scientific	20163
Fast Silver Stain Kit	Beyotime	P0017
BODIPY® 581/591 C11 probe	Thermo Fisher Scientific	D3861
DualLuciferase Reporter Assay System	Promega	E1910
Deposited data		
ShcircEZH2 NOZ metabolome	NGDC database	OMIX006089
circEZH2 RNA pulldown mass spectrometry	NGDC database	OMIX006860
Experimental models: Cell lines		
H69	Eastern Hepatobiliary Surgery Hospital	RRID:CVCL_8121
GBC-SD	Chinese Academy of Sciences	RRID:CVCL_6903
SGC-996	Eastern Hepatobiliary Surgery Hospital	RRID:CVCL_M737
NOZ	JCRB	RRID:CVCL_3079
Experimental models: Organisms/strains		
BALB/c nude mice (nu/nu)	SLAC ANIMAL	N/A
Oligonucleotides		
siRNA sequences, see Table S2	This Paper	N/A
Primers for qPCR, see Table S3	This Paper	N/A
Recombinant DNA		
pLKO.1 vector-puro-shcircEZH2	This Paper	N/A
pmirGLO	Sangon Biotech	N/A
Software and algorithms		
Adobe Photoshop	Adobe	https://www.adobe.com/es/
Graphpad Prism8	GraphPad Prism Software, Inc	https://www.graphpad.com/
SPSS 22.0	IBM	https://www.ibm.com/spss

RESOURCE AVAILABILITY

Lead contact

Further information and requests for resources and reagents should be directed to and will be fulfilled by the Lead Contact, Tang Zhaohui (tzh1236@163.com).

Materials availability

This study did not generate new unique reagents.

Data and code availability

- The datasets used and/or analyzed during the current study are available within the manuscript and its supplemental information files.
- The LC-MS Untargeted Metabonomics data have been deposited in the NGDC database, China National Center for Bioinformation / Beijing Institute of Genomics, Chinese Academy of Sciences (OMIX006089).
- The RNApull down mass spectrometry data have been deposited in the NGDC database, China National Center for Bioinformation / Beijing Institute of Genomics, Chinese Academy of Sciences (OMIX006860).
- Any additional information required to reanalyze the data reported in this paper is available from the lead contact upon request.

EXPERIMENTAL MODEL AND STUDY PARTICIPANT DETAILS

Patients tissue samples

This study enrolled patients diagnosed with GBC and possessing surgical specimens from March 2009 to March 2016 at Xinhua Hospital, affiliated with Shanghai Jiao Tong University School of Medicine. A total of 29 cases of flash-frozen GBC tissues and matched adjacent normal tissues were obtained. All enrolled patients had not undergone preoperative radiotherapy, chemotherapy, or targeted therapy. Tissue

samples were collected immediately after surgical removal and cryopreserved in liquid nitrogen. Patients' information for the GBC cohort is presented in Table S1. Informed consent was obtained from all participants before their involvement in the study. The research protocol adhered to the principles of the Helsinki Declaration and was conducted in accordance with the guidelines provided by the Human Ethics Committee of Xinhua Hospital.

Cell lines culture

The human normal biliary epithelial cell line H69 and human gallbladder cancer cell lines (NOZ, GBC-SD, and SGC- 996) were obtained from Cell Bank of the Chinese Academy of Science (Shanghai, China). Cells were cultured in DMEM (Gibco, USA) supplemented with 10% fetal bovine serum (Gibco, USA). Cells were incubated at 37°C in a 5%CO2 humidified atmosphere. The cells were not cultured for longer than 2 months.

Animal experiments

All animal protocols were approved by the Institutional Animal Care and Use Committee at Xinhua Hospital Affiliated with Shanghai Jiao Tong University School of Medicine and conformed to the Guide for the Care and Use of Laboratory Animals published by the US National Institutes of Health. 4-week male BALB/c nude mice was purchased from Shanghai Laboratory Animal Center of the Chinese Academy of Sciences (Shanghai, China). 1×10^5 NOZ cells transfected by shcircEZH2 or shNC were suspended in 100 μL of PBS and subcutaneously injected into the flank to construct Xenograft experiments (n =5/per group). The tumour volume was evaluated every week, Tumour volume (mm3) = (length) × (width)^2/2. After 4 weeks, mice were euthanized with an intraperitoneal injection of a threefold dose of barbiturates. After that the tumours were weighed and fixed in formalin for further histological analysis immediately.

METHOD DETAILS

Cell transfection

The siRNA against circEZH2, IGF2BP2, si-negative control (si-NC), miR-556 mimic, miR-556 inhibitor, miR-mimic NC and miR-inhibitor NC were synthesized by Ribobio (Guangzhou, China). The target sequences for constructing siRNAs are listed in Table S2. According to the manufacturer's protocol, cell transfection was performed with Lipofectamine 3000 Reagent (Invitrogen, USA). Short hairpin RNAs (shRNAs) against circEZH2 were cloned into a pLKO.1 vector to construct lentiviral particles. The forward sequence of shcircEZH2 is listed in Table S2. After being transfected for 48 h, cells were harvested and assessed by RT-qPCR analysis.

Cell proliferation, colony formation assay

Seed the gallbladder cancer cells (2000 cells in 100ul DMEM per well) in a 96-well plate. After transfection for 1,2,3 days, 10 μL of CCK-8 reagent (Beyotime, China) was added to each well. Then cells were incubated in the dark at 37°C for 2 hours. Measure the absorbance at a wavelength of 450 nm using a microplate reader (BioTek, Winooski, VT, USA).

For colony formation assay, 1000 treated cells were plated in each well of a six-well plate for 8 to 14 days. The cells were fixed with 4% paraformaldehyde and stained with 0.1% crystal violet. After washing and drying the plate, we counted and analyzed the number of cell colonies.

5-Ethynyl-2′-deoxyuridine (EdU) proliferation assay

After seeded in six-well plate overnight, cells were incubated with 10 μM EdU for two hours according to the manufacturer's protocol of BeyoClickTM EdU proliferation assay kit (Beyotime, Shanghai, China), washed with PBS twice for 3-5 minutes each time, remove the wash solution with 1 ml of permeable solution per well. Icubate with endogenous peroxidase blocking solution at room temperature for 20 minutes to inactivate endogenous peroxidase. Then wash with washing solution 3 times for 2 minutes each time. Preparation of Click Reaction Solution according to the manufacturer's protocol. Add 0.5 ml of Click reaction solution to each well and gently shake the culture plate to ensure that the reaction mixture can cover the sample evenly. Incubate at room temperature in the dark for 30 minutes. Add 200 μl of Streptavidin-HRP working solution to the sample and incubate at room temperature for 30 min. Wash with detergent 3 times for 2 minutes each time. Add 0.2ml DAB coloring solution dropwise and incubate at room temperature for 5-30 min. Observe and record under ordinary optical microscope or fluorescence microscope.

Cell cycle detection

Harvested, Washed and Fixed the transfected cells with 70% ethanol at 4°C overnight. The next day, after washed by cold PBS, the cells were stained with 20 μg/ml Propidium iodide (PI; Beyotime, China) and 100 μg/ml RNase A at 37°C for 30 min. Cell cycle was examined by flow cytometry using the FACS Calibur system (BD Biosciences, USA).

Immunohistochemistry (IHC), Fluorescence *in situ* hybridization (FISH)

xenograft tumour issues or clinicopathological tissue were fixed with 4% paraformaldehyde and then embedded in paraffin and cut into slices. Paraffin-embedded sections were dewaxed with xylene and hydrolyzed in a graded ethanol series. Then, sections were immersed in 3%

hydrogen peroxide for 10 min and incubated with primary antibodies overnight at 4°C, followed by incubating with secondary antibodies for 1h at room temperature. DAB complex was used to visualize the targeted molecules and hematoxylin was used to counterstain nuclei. Images were captured at identical exposure conditions using a microscope (Leica, Germany). For each slide, 5 high magnification (×200) field were collected under a light microscope. The following primary antibodies were used: cyclinD1 (1:100 dilution, Abclonal, China), Ki-67(1:100 dilution, Cell Signaling Technology, USA), GPX4 (1:100 dilution, Proteintech, China), SCD1 (1:100 dilution, ABclonal, China), IGF2BP2 (1:100 dilution, Proteintech, China).

For Fluorescence *in situ* hybridization (FISH), NOZ and SGC-996 Cells were seeded in six-well plate overnight. The cells were fixed with 4% paraformaldehyde and washed with PBS for 30 min twice. biotin-labeled CircEZH2 probe was designed and synthesized by Servicebio (cir-cEZH2: 5'- GGCCCATGATTATTCTCCCTAGTCCCGCGC-3'). FISH assay was performed under RNase-free conditions. After hybridization with specific FISH probes overnight in a dark moist chamber, cells were washed with PBS three times. Then incubated with the reagents in Alexa FluorTM 488 Tyramide SuperBoost™ Kits (Thermo Fisher Scientific, Waltham, USA). Images were detected using a fluorescence microscope (OLYMPUS, Tokyo, Japan).

Actinomycin D assays

NOZ cell line was seeded in 6cm dish (3 × 10^6 cells). 24 hours later, cells were treated by 2 μg/ml Actinomycin D (Sigma) and collected at indicated time points. RT-qPCR was used to analyse the RNA stability.

RNA extraction and RT-qPCR analysis

According to the manufacturer's instructions, total RNA derived from GBC cell lines and tissues was extracted using TRIzol reagent (TaKaRa, Japan). The cDNAs were synthesized from total RNA using a PrimeScript™ RT Master Mix (Perfect Real Time) (TaKaRa, Japan). U6 and beta-actin (ACTB) were utilized as controls. RT-qPCR was performed with The Hieff UNICON® qPCR SYBR® Green Master Mix (Yeasen, Shanghai, China) according to its instruction. the 2$^{-\Delta\Delta Ct}$ method were applied to analyze the quantitate mRNA or miRNA expression. All primers were purchased from Sangon Biotech (Shanghai, China. The primer sequences are listed in Table S3.

RNase R treatment

The total RNA was divided into two groups: one for RNase R (Geneseed, Guangzhou, China) treatment and the other for control. The treated group total RNA was incubated with 5 U/μg RNase R (Geneseed, Guangzhou, China) for 30 min at 37°C, and then analyzed by RT-qPCR according to the protocol.

Western blotting assays

The extraction of total protein was prepared using RIPA buffer (Beyotime, China) and protease inhibitor cocktail (Yeasen, China). Equal amounts of total protein extraction were separated by SDS-polyacrylamide gel electrophoresis (SDS-PAGE) and then transferred onto a 0.22μm PVDF membrane (Millipore, USA). After blocked with 5% skimmed milk for 1h, the membrane was incubated with primary antibodies against GPX4 (1:1000 dilution, Proteintech, China), NRF2 (1:1000, Cell Signaling Technology, USA), SCD1 (1:1000 dilution, ABclonal, China), IGF2BP2 (1:1000, Proteintech, China), AGO2 (1:1000 dilution, Abacam, USA) , GAPDH (1:2000 dilution, Cell Signaling Technology, USA), ubiquitin (1:2000 dilution, Proteintech, China), and ACTB (1:2000 dilution, Proteintech, China) overnight at 4°C. The next day, membrane was incubated with secondary antibodies for 1 hours, and protein bands were detected using the ECL detection system (Amersham Biosciences, Buckinghamshire, UK).

LC-MS Untargeted Metabonomics

All chemicals and solvents were analytical or HPLC grade. 1 mL methanol: water (4/1, vol/vol) and 200 μL chloroform were added to each sample. Pipette and ultrasonic homogenizer were used to break up the cells for 3 min at 500 w. The above mixtures and 20 μL of L-2-chlorophenylalanine (0.06mg / mL) of each sample were transferred to 1.5 mL Eppendorf tubes. The samples were centrifuged at 13000rpm for 10min after 20min of ultrasonic extraction. 800 μL of supernatant was dried in a freeze concentration centrifugal dryer. After adding 300μL mixture of methanol and water (1/4, vol/vol), samples were vortexed for 30 s and extracted by ultrasonic for 3 min. Then samples were centrifuged at 4°C (13,000 rpm) for 10 min. The supernatants (150μL) from each tube were collected and filtered through 0.22 μm micro-filters. The collection then transferred to LC vials and stored at -80°C until LC -MS analysis. A quality control sample was prepared by mixing aliquot of the all samples to be a pooled sample.

ACQUITY UPLC I-Class system (Waters Corporation, Milford, USA) coupled with Q-Exactive quadrupole-Orbitrap mass spectrometer equipped with heated electrospray ionization (ESI) source (Thermo Fisher Scientific, Waltham, MA, USA) was used to analyse the metabolic profiling in both ESI positive and ESI negative ion modes. The original LC-MS data were processed by software Progenesis QI V2.3 (Nonlinear, Dynamics, Newcastle, UK) for baseline filtering, peak identification, integral, retention time correction, peak alignment, and normalization.

The LC-MS Untargeted Metabonomics data have been deposited in the NGDC database, China National Center for Bioinformation / Beijing Institute of Genomics, Chinese Academy of Sciences (OMIX006089).

miRNA pull down

Streptavidin-coupled Dynabeads (Invitrogen) were washed, resuspended in the buffer. The biotin-labelled miR-556-5p probe (GAUGAGCUCAUUGUAAUAUGAG) or control probe was designed and synthesized by GenePharm (Shanghai, China). 10cm dish of NOZ cells were transfected with 100 nM of probe overnight. Wash, lyse and centrifuge the above NOZ cells to obtain the extraction. Then the extraction was added to Streptavidin-coupled Dynabeads. After incubating at room temperature for 10 min, the beads were separated with a magnet for 2 min. Wash the beads with PBS twice. The pulled-down RNA was extracted by Trizol reagent and followed by RT-qPCR analysis.

RNA pull-down assay, silver staining and mass spectrometry analysis

Plasmid containing two T7 promoters and circEZH2, constructed by Genechem (Shanghai, China), was digested using a restriction endonuclease. The sense and antisense oilgo were transcribed with T7 High Yield RNA Transcription Kit (Vazyme, Nanjing, China), which were then purified using the RNeasy Mini Kit (Qiagen, Germany). The Pierce™ RNA 3′ End Desthiobiotinylation Kit (Thermo Fisher Scientific, USA) was used to label biotin to the 3′ end of RNA to construct the sense and antisense probe.

1×10^7 cells were lysed in 1000 μl IP lysis buffer (Thermo Scientific, USA) supplemented with a cocktail of proteinase inhibitors, RNase inhibitors and phosphatase inhibitors (Invitrogen, USA), and then incubated with 5 μg biotinylated probes for two hours. A total of 100 μl prepared streptavidin magnetic beads (Thermo Fisher Scientific, USA) were added to each binding reaction and further incubated for another hour at room temperature. The beads were briefly washed five times with elution buffer. Finally, SDS-PAGE Sample Loading Buffer (Beyotime, China) was used to retrieve the binding proteins for further mass spectrometry or western blot analysis. Fast Silver Stain Kit (Beyotime, Shanghai, China) was used to silver stain the pulldown protein according to the manufacturer's instructions, while mass spectrometry analysis was performed by BGI Genomics (Shenzhen, China).

The RNApull down mass spectrometry data have been deposited in the NGDC database, China National Center for Bioinformation / Beijing Institute of Genomics, Chinese Academy of Sciences (OMIX006860).

Lipid peroxidation detection

Dilute the BODIPY® 581/591 C11 probe (Invitrogen, Carlsbad, CA, USA) in PBS at a 1:1000 ratio and add it to the transfected cells, then incubate for 30 minutes at 37°C in dark. Digest and wash the cells with PBS, resuspend the pellet cells in 200 μL PBS, and detect by FACS Calibur system (BD Biosciences, San Jose, CA, USA) at FITC channel.

Co-immunoprecipitation

To detect the extent of ubiquitination modification of IGF2BP2, 10cm dish transfected cells were lysed in 500 μl co-IP buffer supplemented with a cocktail of proteinase inhibitors. The lysates were divided into two equal parts and each part was added IgG or IGF2BP2 antibody. After incubation at 4°C overnight, equal Protein A+G Agarose beads (Beyotime, Shanghai, China) were added to the lysates and shaken slowly at 4°C for 2 h. After that, beads were washed 5 times with PBS. SDS sample buffer was added to the agarose beads for further western blot analysis.

Luciferase reporter assays

The wide type (WT) circEZH2 or SCD1 3′-untranslated region (UTR) containing miR-556-5p targeting sequence and the mutated type (MUT) was amplified and constructed into the luciferase reporter plasmid pmirGLO (Sangon Biotech, Shanghai). After transfecting the constructed plasmid into the cells for 24 hours, miR-556-5p mimics and negative controls were transfected into the cells. The cells were further incubated for an additional 24 hours before being collected and moderately lysed. Luciferase activities were measured using the DualLuciferase Reporter Assay System (Promega, USA). The relative luciferase activity was normalized against to the Renilla luciferase activity.

Ethics approval and consent to participate

The present study was approved by the Ethics Committee of Xinhua Hospital. Written informed consent was obtained from all the patients, and the study was conducted in accordance with the Declaration of Helsinki.

QUANTIFICATION AND STATISTICAL ANALYSIS

All statistical analyses were performed using GraphPad Prism (GraphPad Software, Inc. La Jolla, USA) and SPSS 22.0 (IBM Corp.,Armonk, NY, USA). The data were presented as mean ± SD, and compared by Student's t test or ANOVA with Tukey test. Fisher's exact test was used to determine the association between the expression of circEZH2 with GBC patients' clinic pathological parameters. Statistical significance was set at $P < 0.05$. *$P < 0.05$. ns., not significant.

ADDITIONAL RESOURCES

The datasets used and/or analyzed during the current study are available from the corresponding author on reasonable request.